

## $E_p$ – $E_{iso}$ CORRELATION IN A MULTIPLE SUBJET MODEL OF GAMMA-RAY BURSTS

KENJI TOMA<sup>1</sup>, RYO YAMAZAKI<sup>2</sup> AND TAKASHI NAKAMURA<sup>1</sup>

<sup>1</sup>Department of Physics, Kyoto University, Kyoto 606-8502, Japan

<sup>2</sup>Department of Earth and Space Science, Osaka University, Toyonaka 560-0043, Japan

*Draft version November 26, 2018*

### ABSTRACT

We perform Monte Carlo simulations to study  $E_p$ – $E_{iso}$  correlation in the context of a multiple subjet model (or inhomogeneous jet model) for gamma-ray bursts (GRBs), X-ray-rich GRBs (XRRs), and X-ray flashes (XRFs). For a single subjet, we find that  $E_p \propto E_{iso}^{0.4}$  for large viewing angles. For the multiple subjet model in which all the subjets have the same intrinsic properties, off-axis events show  $E_p \propto E_{iso}^a$  with  $0.4 < a < 0.5$ . If the intrinsic properties of the subjets are distributed so that on-axis emission of each subjet follows a correlation  $E_p \propto L_{iso}^{1/2}$ , we obtain the Amati correlation ( $E_p \propto E_{iso}^{1/2}$ ) over three orders of magnitude in  $E_p$ . Although the scatter around the Amati correlation is large in the simulation, the results are consistent with the observed properties of GRBs with known redshifts and the BASTE GRBs with pseudo redshifts derived from the lag–luminosity correlation. We also calculate the event rates, the redshift distributions, and the  $T_{90}$  duration distributions of GRBs, XRRs, and XRFs which can be detected by *HETE-2*, assuming that the source redshift distribution is in proportion to the cosmic star formation rate. It is found that the event rates of three classes are comparable, that the average redshift of the XRRs is a little larger than those of the GRBs and the XRFs, and that short XRRs arise when a single subjet is viewed off-axis or viewed on-axis with slightly high redshift.

*Subject headings:* gamma rays: bursts — gamma rays: theory

### 1. INTRODUCTION

*HETE-2* observations have provided strong evidence that softer and dimmer gamma-ray bursts (GRBs) smoothly extend to X-ray flashes (XRFs) through an intermediate class of events called X-ray-rich GRBs (XRRs). For events with known redshifts and well observed spectra, the rest-frame spectral peak energy  $E_p$  and the “bolometric” isotropic-equivalent  $\gamma$ -ray energy  $E_{iso}$  have a strong correlation, i.e.,  $E_p \propto E_{iso}^{1/2}$  (Amati et al. 2002). This  $E_p$ – $E_{iso}$  correlation, called the Amati correlation, has recently been extended down to lower energies characteristic of XRFs (Lamb et al. 2004). Since various observed quantities other than the Amati correlation also distribute continuously among GRBs, XRRs, and XRFs (Sakamoto et al. 2005), it is strongly suggested that these three classes are related phenomena.

While many different models have been proposed for XRFs (see Granot, Ramirez-Ruiz, & Perna 2005, and references therein), we have proposed the “off-axis model” (Yamazaki, Ioka, & Nakamura 2002, 2003) in which XRFs are the usual GRB jets viewed from an off-axis viewing angle (see also Woods & Loeb 1999). When the jet is observed off-axis, the emitted photons are out of the beaming cone and less blueshifted than photons emitted along the jet axis, so that the events look like XRFs. It has been shown that the viewing angle of the jet is the key parameter to understand the various properties of the GRBs and that the luminosity–variability/lag/width correlations might be naturally derived in the framework of off-axis models (Ioka & Nakamura 2001).

As for the Amati correlation, Yamazaki, Ioka, & Nakamura (2004a) computed  $E_p$  and  $E_{iso}$  using the uniform jet model and found that the results are compatible with the observations. They also found that  $E_p \propto E_{iso}^{1/3}$  in the smaller  $E_{iso}$  regime. Eichler & Levinson (2004) investigated the correlation in an

annular jet model, and derived that if the viewing angles are within the annulus,  $E_p \propto E_{iso}^a$  with  $1/3 < a < 1/2$ , which is compatible with the observations. Compared with our uniform jet model, in the annular jet model the energy is large due to the emissions from widely distributed segments with similar viewing angles. Eichler & Levinson (2004) also anticipated that multiple discrete emissions could have the same effect.

The off-axis jet model has recently been improved to include short GRBs (Yamazaki, Ioka, & Nakamura 2004b) as a unified model, where the GRB jet is not uniform but made up of multiple subjets or multiple emission patches. This is an extreme case of an inhomogeneous jet model (Nakamura 2000; Kumar & Piran 2000). The crucial parameter is the multiplicity,  $n_s$ , of the subjets along the line of sight. If  $n_s \geq 2$ , the burst looks like a long GRB, and if  $n_s = 1$  the burst looks like a short GRB, while if  $n_s = 0$  the burst is an off-axis event for all the subjets and looks like an XRF or an XRR. We also found that the unified model may explain the bimodal distribution of the  $T_{90}$  durations of BATSE GRBs (Toma, Yamazaki, & Nakamura 2005).

In this paper, we examine  $E_p$ – $E_{iso}$  correlation in the multiple subjet model to show that the unified model is consistent with the observations of  $E_p$  and  $E_{iso}$ . This paper is organized as follows. In § 2, we describe our multiple subjet model for prompt emissions. First, the  $E_p$ – $E_{iso}$  correlation for a single subjet is discussed in § 3, and then we discuss the results of Monte Carlo simulations in the multiple subjet model in § 4. Section 5 is devoted to discussion.

### 2. PROMPT EMISSION MODEL

Let us suppose that  $N_{tot}$  subjets with opening half-angle  $\Delta\theta_{sub}^{(j)}$  are launched from the central engine of GRB randomly in time and directions and that the whole jet with opening half-angle  $\Delta\theta_{tot}$  consists of these subjets. We introduce the spherical coordinate system  $(r, \vartheta, \varphi)$  in the central engine frame, where the origin is the location of the central engine,

arXiv:astro-ph/0504624v2 22 Aug 2005

and  $\vartheta = 0$  is the axis of the whole jet. The axis of the  $j$ th subset ( $j = 1, \dots, N_{\text{tot}}$ ) is denoted by  $(\vartheta^{(j)}, \varphi^{(j)})$ . If the direction of the observer is given by  $(\vartheta_{\text{obs}}, \varphi_{\text{obs}})$ , the viewing angle of the  $j$ th subset from the line of sight is

$$\theta_v^{(j)} = \cos^{-1}[\sin \vartheta_{\text{obs}} \sin \vartheta^{(j)} \cos(\varphi_{\text{obs}} - \varphi^{(j)}) + \cos \vartheta_{\text{obs}} \cos \vartheta^{(j)}]. \quad (1)$$

For emission model of each subset, we use the same formulations and notations as used in Yamazaki, Ioka, & Nakamura (2003). Let us use another spherical coordinate system  $(r, \theta, \phi)$  in the central engine frame, where the origin is the location of the central engine, and  $\theta = 0$  is the line of sight. We adopt an instantaneous emission, at  $t = t_0^{(j)}$  and  $r = r_0^{(j)}$ , of an infinitesimally thin shell moving with the Lorentz factor  $\gamma_{(j)}$ . Then one can obtain the formula of the observed flux from the  $j$ th subset with viewing angle  $\theta_v^{(j)}$  at frequency  $\nu$  and time  $T$ ,

$$F_\nu^{(j)}(T) = \frac{2(1+z)r_0^{(j)}cA^{(j)}}{d_L^2} \frac{\Delta\phi^{(j)}(T)f^{(j)}[(1+z)\nu\gamma_{(j)}(1-\beta^{(j)}\cos\theta(T))]}{\gamma_{(j)}^2(1-\beta^{(j)}\cos\theta(T))^2}, \quad (2)$$

where  $z$  and  $d_L$  are the redshift and the luminosity distance of the source, respectively;  $f^{(j)}(\nu')$  and  $A^{(j)}$  represent the spectral shape and the amplitude of the emission in the comoving frame, respectively. Here  $T = 0$  is chosen as the time of arrival at the observer of a photon emitted at the origin at  $t = 0$ . The set of points that emit photons observed at a given time  $T$  is an arc (or a circle). The functions  $\theta(T)$  and  $\Delta\phi^{(j)}(T)$  represent an angular radius and a central angle of the arc, respectively:

$$\cos\theta(T) = \frac{c}{r_0^{(j)}} \left( t_0^{(j)} - \frac{T}{1+z} \right), \quad (3)$$

$$\Delta\phi^{(j)}(T) = \begin{cases} \pi, & \text{(for } \theta_v^{(j)} < \Delta\theta_{\text{sub}}^{(j)} \text{ and } 0 < \theta(T) < \Delta\theta_{\text{sub}}^{(j)} - \theta_v^{(j)}), \\ \cos^{-1} \left( \frac{\cos\Delta\theta_{\text{sub}}^{(j)} - \cos\theta_v^{(j)}\cos\theta(T)}{\sin\theta_v^{(j)}\sin\theta(T)} \right), & \\ \text{(for otherwise).} & \end{cases} \quad (4)$$

Equation (3) can be rewritten by

$$1 - \beta^{(j)}\cos\theta(T) = \frac{1}{r_0^{(j)}/c\beta^{(j)}} \left( \frac{T}{1+z} - t_{\text{dep}}^{(j)} \right), \quad (5)$$

where  $t_{\text{dep}}^{(j)} = t_0^{(j)} - r_0^{(j)}/c\beta^{(j)}$  is the departure time from the central engine of the  $j$ th subset.

The observed spectrum of GRBs is well approximated by the Band spectrum (Band et al. 1993). In order to have a spectral shape similar to the Band spectrum, we adopt the following form of the spectrum in the comoving frame,

$$f^{(j)}(\nu') = \begin{cases} (\nu'/\nu_0^{(j)})^{1+\alpha_B^{(j)}} \exp(-\nu'/\nu_0^{(j)}) & \text{(for } \nu'/\nu_0^{(j)} \leq \alpha_B^{(j)} - \beta_B^{(j)}), \\ (\nu'/\nu_0^{(j)})^{1+\beta_B^{(j)}} (\alpha_B^{(j)} - \beta_B^{(j)})^{\alpha_B^{(j)} - \beta_B^{(j)}} \exp(\beta_B^{(j)} - \alpha_B^{(j)}) & \text{(for } \nu'/\nu_0^{(j)} \geq \alpha_B^{(j)} - \beta_B^{(j)}, \end{cases} \quad (6)$$

where  $\nu_0^{(j)}$ ,  $\alpha_B^{(j)}$ , and  $\beta_B^{(j)}$  are the break frequency and the low- and high-energy photon index, respectively.

As a summary, equations (2), (4), (5), and (6) are the basic equations to calculate the observed flux from each subset, which depends on the following parameters:  $\theta_v^{(j)}$  (which is determined by  $\vartheta^{(j)}$ ,  $\varphi^{(j)}$ ,  $\vartheta_{\text{obs}}$ , and  $\varphi_{\text{obs}}$  through equation (1)),  $\Delta\theta_{\text{sub}}^{(j)}$ ,  $\gamma^{(j)}$ ,  $t_{\text{dep}}^{(j)}$ ,  $r_0^{(j)}$ ,  $\alpha_B^{(j)}$ ,  $\beta_B^{(j)}$ ,  $\nu_0^{(j)}$ ,  $A^{(j)}$ , and  $z$ . The whole light curve from the GRB jet is produced by the superposition of the emissions from the subsets.

### 3. $E_p$ - $E_{\text{ISO}}$ CORRELATION FOR A SINGLE SUBJECT

Before examining  $E_p$ - $E_{\text{ISO}}$  correlation for the multiple subset model, it is instructive to calculate  $E_p$ - $E_{\text{ISO}}$  correlation when a single subset is seen off-axis. Using equations (2), (4), (5), and (6) for  $N_{\text{tot}} = 1$  and a given  $\theta_v$ , we compute the peak energy of the time-integrated spectrum measured in the cosmological rest frame,  $E_p$ , and the ‘‘bolometric’’ isotropic-equivalent energy,  $E_{\text{ISO}}^s$ , integrating over the  $1 - 10^4$  keV range in the cosmological rest frame. Here the superscript  $s$  of  $E_{\text{ISO}}^s$  means ‘‘single’’. We adopt the following subset parameters:  $\Delta\theta_{\text{sub}} = 0.02$  rad,  $\gamma = 300$ ,  $\alpha_B = -1$ ,  $\beta_B = -2.5$ , and  $\gamma h\nu_0' = 350$  keV. In Figure 1, we show  $E_p$  and  $E_{\text{ISO}}^s$  (in units of  $2.8 \times 10^3 \pi A r_0^2$ ) for  $0 < \theta_v < 0.1$  rad (the solid line). The dashed and dot-dashed lines are  $E_{\text{ISO}}^s 0.4$  and  $E_{\text{ISO}}^s 1/3$ , respectively. We see that for  $\theta_v > \Delta\theta_{\text{sub}}$ , as  $\theta_v$  increases, both  $E_p$  and  $E_{\text{ISO}}^s$  decreases. We focus on small  $E_{\text{ISO}}^s$  regime. At first the  $E_p$ - $E_{\text{ISO}}^s$  correlation approaches  $E_p \propto E_{\text{ISO}}^s 0.4$ , but for even larger  $\theta_v$ ,  $E_p \propto E_{\text{ISO}}^s 1/3$ . This behavior is explained as follows. Firstly the spectral peak energy scales as  $E_p \propto [1 - \beta \cos(\theta_v - \Delta\theta_{\text{sub}})]^{-1}$  because of the Doppler effect, and for large  $\theta_v$ ,  $E_p \propto \theta_v^{-2}$ . Next we compute  $E_{\text{ISO}}^s$  by integrating equation (1) over  $\nu$  and  $T$ , and study its dependence on  $\theta_v$ . When  $\theta_v$  is large but  $E_p$  is in the  $1 - 10^4$  keV range, the integration over  $\nu/(1+z)$  results in a constant depending on the Band spectral parameters and another Doppler factor  $[1 - \beta \cos\theta(T)]^{-1}$ . As for the integration with respect to  $T$ , we change the variable from  $T$  to  $\theta(T)$ , and obtain:

$$E_{\text{ISO}}^s \propto \int_{\theta_v - \Delta\theta_{\text{sub}}}^{\theta_v + \Delta\theta_{\text{sub}}} \frac{\Delta\phi(\theta) \sin\theta d\theta}{(1 - \beta \cos\theta)^3}. \quad (7)$$

For large  $\theta_v$ ,  $\Delta\phi \simeq \Delta\theta_{\text{sub}}/\theta_v$ , so that  $E_{\text{ISO}}^s \propto \theta_v^{-1} [1 - \beta \cos(\theta_v - \Delta\theta_{\text{sub}})]^{-2} - [1 - \beta \cos(\theta_v + \Delta\theta_{\text{sub}})]^{-2} \simeq \theta_v^{-1} [1 - \beta \cos(\theta_v - \Delta\theta_{\text{sub}})]^{-2} \propto E_p^{2.5}$ . When  $\theta_v$  is even so large as  $E_p \sim 1$  keV, the integration over  $\nu/(1+z)$  results in a factor  $(1 - \beta \cos\theta)^{1+\beta_B}$ , so that the same calculation gives us  $E_{\text{ISO}}^s \propto \theta_v^{-1} [1 - \beta \cos(\theta_v - \Delta\theta_{\text{sub}})]^{\beta_B} \propto E_p^3$  for  $\beta_B = -2.5$ .

For a single subset, off-axis events obey  $E_p \propto E_{\text{ISO}}^{0.4}$  for small  $E_p$  regime (but  $E_p > 1$  keV). The index of the  $E_p$ - $E_{\text{ISO}}$  correlation,  $a = 0.4$ , is obtained irrespective of the intrinsic subset parameters  $\Delta\theta_{\text{sub}}$ ,  $\gamma$ ,  $t_{\text{dep}}$ ,  $r_0$ ,  $\alpha_B$ ,  $\beta_B$ ,  $\nu_0'$ , and  $A$ , as can be seen in the above derivation.

### 4. $E_p$ - $E_{\text{ISO}}$ CORRELATION IN THE MULTIPLE SUBJECT MODEL

Let us perform Monte Carlo simulations to derive  $E_p$ - $E_{\text{ISO}}$  correlation in the multiple subset model. For simplicity, we generate one GRB jet with opening half-angle  $\Delta\theta_{\text{tot}} = 0.3$  rad and random 5000 lines of sight of the observer with  $0 < \vartheta_{\text{obs}} < 0.35$  rad according to the probability distribution of  $\sin\vartheta_{\text{obs}} d\vartheta_{\text{obs}} d\varphi_{\text{obs}}$ . Then, for each observer, we calculate the peak energy of the time-integrated spectrum measured in the cosmological rest frame,  $E_p$ , and the ‘‘bolometric’’ isotropic-equivalent energy,  $E_{\text{ISO}}$ , integrating over the  $1 - 10^4$  keV range in the cosmological rest frame. The departure time of each subset  $t_{\text{dep}}^{(j)}$  is assumed to be homogeneously random between  $t = 0$  and  $t = t_{\text{dur}}$ , where  $t_{\text{dur}}$  is the active time of the central engine measured in its own frame, and  $t_{\text{dur}} = 20$  s is adopted. The central engine is assumed to produce  $N_{\text{tot}} = 350$  subsets following the angular distribution function

$$\frac{dN}{d\Omega} \propto \begin{cases} 1, & 0 < \vartheta^{(j)} < \vartheta_c, \\ (\vartheta^{(j)}/\vartheta_c)^{-2}, & \vartheta_c < \vartheta^{(j)} < \vartheta_b, \end{cases} \quad (8)$$

where  $\vartheta_b = \Delta\theta_{tot} - \Delta\theta_{sub}$ , and  $\vartheta_c = 0.03$  rad. This corresponds to the universal structured jet model (see Rossi, Lazzati, & Rees 2002; Zhang & Mészáros 2002a). The angular distribution of the subjets in our simulations is shown in Figure 2. The solid circle describes each subjet and the dashed circle describes the whole jet. The meaning of plus sign will be discussed later. We assume that all the subjets have the same values of the following parameters:  $\Delta\theta_{sub}^{(j)} = 0.02$  rad,  $\gamma_{(j)} = 300$ ,  $r_0^{(j)} = 3.0 \times 10^{14}$  cm,  $\alpha_B^{(j)} = -1$ , and  $\beta_B^{(j)} = -2.5$ . The intrinsic spectral parameter  $\gamma h\nu_0^{(j)}$  and the amplitude  $A^{(j)}$  are determined so that the time-averaged emission from a single subjet viewed *on-axis* satisfies the following correlation,

$$\frac{L_{iso}^s}{10^{52} \text{ erg s}^{-1}} = \xi \left( \frac{E_p^s}{1 \text{ keV}} \right)^2, \quad (9)$$

where  $L_{iso}^s$  is the time-averaged ‘‘bolometric’’ isotropic-equivalent luminosity and  $E_p^s$  is the time-averaged rest-frame spectral peak energy of the *on-axis* emission from a single subjet. As for the validity of this correlation, Liang, Dai, & Wu (2004) argue that for long bright BATSE GRBs the observed  $\gamma$ -ray flux  $F$  is correlated with the observed time-resolved  $E_p^{obs}$  at each time in a similar way, i.e.,  $F \propto (E_p^{obs})^2$ , which supports the assumption that the on-axis emission of each subjet obeys this correlation. Lloyd-Ronning & Ramirez-Ruiz (2002) show that there is a positive correlation between  $\gamma$ -ray luminosity and time-resolved rest-frame spectral peak energy by using variability-luminosity correlation (see also Yonetoku et al. 2004; Ghirlanda et al. 2005b). This correlation could be obtained by standard synchrotron internal shock model (e.g., Zhang & Mészáros 2002b). However, the coefficient  $\xi$  is highly uncertain. Therefore we chose the values of  $\xi$  so that the results of simulations reproduce the observations. We consider two cases of  $\gamma h\nu_0^{(j)}$  and  $A^{(j)}$ : Case (i)  $\gamma h\nu_0^{(j)}$  and  $\xi$  are fixed as 350 keV and  $6.0 \times 10^{-5}$ , respectively, for all  $j$ . Case (ii)  $\gamma h\nu_0^{(j)}$  and  $\xi$  are distributed around the above values.

#### 4.1. Case (i)

Let us consider the Case (i) as a simple toy model, in which all the subjets have the same intrinsic parameters, so that we can investigate the pure kinematical effects from the multiple discrete emission patches. The results are shown in Figure 3. The black solid line shows the  $E_p$ - $E_{iso}$  correlation for a single subjet derived with the same parameters. We see that the black solid line traces the left-side edge of the distribution of the simulated bursts. When a single subjet is seen on-axis, the time-averaged spectral peak energy  $E_p^s = g_n h\nu_0' / \gamma(1-\beta) \approx 2g_n \gamma h\nu_0' \sim 500$  keV, where a numerical factor  $g_n (\sim 0.7)$  comes from the contribution of soft emission from the whole subjet, while  $g_n = 1$  in the case of point source approximation. The observed pulse has a duration determined by the angular spreading time as  $\delta T = r_0 \Delta\theta_{sub}^2 / 2c = 2$  s. Then, according to equation (9),  $L_{iso}^s \simeq 1.5 \times 10^{53}$  ergs  $s^{-1}$ , so that  $E_{iso}^s = L_{iso}^s \delta T \simeq 3 \times 10^{53}$  ergs. This corresponds to  $E_p$  reaching its maximum around  $E_{iso} \sim 3 \times 10^{53}$  ergs. When more than 1 subjet are seen on-axis, i.e.,  $n_s \geq 2$ ,  $E_p$  is the same as in the case of  $n_s = 1$ , but  $E_{iso} \simeq n_s E_{iso}^s$ . The maximum value of multiplicity  $n_s$  is about 30, when the line of sight is along the center of the whole jet. Then  $E_{iso}$  takes the maximum value of  $\simeq 10^{55}$  ergs. Points with  $E_p < 500$  keV correspond to the case of  $n_s = 0$ , in which all the subjets are

seen off-axis, i.e.,  $\theta_v^{(j)} > \Delta\theta_{sub}$  for all  $j$ . For each line of sight, the observed flux is dominated by the emission of the subjets with small  $\theta_v^{(j)}$ . Thus  $E_p$  is determined by the minimum value of  $\theta_v^{(j)}$ ,  $\theta_v^{min}$ . Let  $n_s^{off}$  be the number of the subjets with  $\theta_v^{(j)}$  around  $\theta_v^{min}$ . When  $n_s^{off} = 1$ , the observed flux is dominated by a single subjet, and the  $\theta_v^{min}$ -dependence of  $E_p$  and  $E_{iso}$  is determined as discussed in § 3. Such points are on the black solid line. When  $n_s^{off} \geq 2$ , for each  $\theta_v^{min}$ ,  $E_p$  is the same as for the case of  $n_s^{off} = 1$ , but  $E_{iso} \simeq n_s^{off} E_{iso}^s$ . Thus the scatter of the simulated points for  $E_p < 500$  keV arises from that of  $n_s^{off}$ . We find that the right-side edge of the distribution of the points follows  $E_p \propto E_{iso}^{1/2}$ . The reason for this behavior is as follows. For each  $\theta_v^{min}$ ,  $E_p \propto [1 - \beta \cos(\theta_v^{min} - \Delta\theta_{sub})]^{-1}$ . The other quantity  $E_{iso}$  is given for the largest  $n_s^{off}$ . Since the probability that these  $n_s^{off}$  subjets have the same axis ( $\vartheta^{(j)}, \varphi^{(j)}$ ) is quite low, they should be smoothly distributed around the line of sight. Then in calculating  $E_{iso}$  by equation (7) for the multiple subjets case, we can take  $\Delta\phi \simeq \pi$ . Therefore, for each  $\theta_v^{min}$ ,  $E_{iso} \propto [1 - \beta \cos(\theta_v^{min} - \Delta\theta_{sub})]^{-2}$ , and then we obtain  $E_{iso} \propto E_p^2$ . Such situation resembles the case of the annulus jet model in which the line of sight is inside the annulus and the inner radius of the annulus changes (see Eichler & Levinson 2004).

For a multiple subjet model, off-axis events (with  $n_s = 0$ ) follows  $E_p \propto E_{iso}^a$  with  $0.4 < a < 0.5$ . This range of  $a$  is obtained irrespective of the intrinsic subjet parameters  $\Delta\theta_{sub}$ ,  $\gamma$ ,  $t_{dep}$ ,  $r_0$ ,  $\alpha_B$ ,  $\beta_B$ ,  $\nu_0'$ , and  $A$ .

#### 4.2. Case (ii)

We here assume that  $\gamma h\nu_0^{(j)}$  is distributed randomly according to a lognormal distribution function (Ioka & Nakamura 2002) with an average of  $\log(350 \text{ keV})$  and a logarithmic variance of 0.2. For given  $\gamma h\nu_0^{(j)}$ ,  $A^{(j)}$  is determined by equation (9). The coefficient  $\xi$  is also assumed to obey a lognormal distribution with an average of  $-5 + \log(6.0)$  and a logarithmic variance of 0.15. The other parameters of the subjets are fixed to the same values as in the previous simulation. We calculate  $E_{iso}$  and  $E_p$ , and then assign a redshift for each observer to calculate the distance and the observed lightcurve. The source redshift distribution is assumed to be in proportion to the cosmic star formation rate. We adopt the model SF2 in Porciani & Madau (2001), in which we take the standard cosmological parameters of  $H_0 = 70 \text{ km s}^{-1} \text{ Mpc}^{-1}$ ,  $\Omega_M = 0.3$ , and  $\Omega_\Lambda = 0.7$ . Finally, we select detectable events with observed peak photon fluxes in the  $1 - 10^4$  keV band larger than  $1.0 \text{ ph cm}^{-2} \text{ s}^{-1}$ , which corresponds to the threshold sensitivity of *HETE-2* (see Band et al. 2003; Lamb, Donaghy, & Graziani 2005). Figure 4 shows the result of our simulation. Plus signs represent bursts that can be detected by *HETE-2*, while crosses represent ones that cannot be detected. They are compared with the *BeppoSAX* and *HETE-2* data (points with error bars) taken from Ghirlanda, Ghisellini, & Lazzati (2004). The solid line represents the best fitted line for 442 GRBs with redshifts estimated by the lag-luminosity correlation (Ghirlanda, Ghisellini, & Firmani 2005a). We see that our simulated GRBs cover the observed GRBs over three orders of  $E_p$ , so that our multiple subjet model with the intrinsic correlation  $E_p^s \propto L_{iso}^s{}^{1/2}$  under the universal structured jet model is consistent with the observations.

The  $n_s = 1$  bursts directly reflect the assumed correlation of  $E_p^s \propto L_{iso}^s{}^{1/2}$ . For larger  $n_s$ ,  $E_{iso}$  becomes larger, and  $E_p$  is de-

terminated by the subjet emission with the largest  $L_{iso}^s$  observed. As a result, all the simulated bursts roughly obeys  $E_p \propto E_{iso}^{1/2}$  over about three orders of magnitude in  $E_p$ . The scatter comes from the differences of the number of the observed subjets and the differences of the parameters of each subjet.

### 5. DISCUSSION

We have investigated  $E_p$ - $E_{iso}$  correlation in a multiple subjet model for GRBs, XRRs, and XRFs. We find that off-axis events (with  $n_s = 0$ ) for multiple discrete emission regions show  $E_p \propto E_{iso}^a$  with  $0.4 < a < 0.5$ . It is assumed that the subjet parameters  $\gamma h\nu_0^{(j)}$  and  $A^{(j)}$  are distributed so that emission of the subjets viewed on-axis follows the correlation  $E_p^s \propto L_{iso}^s{}^{1/2}$ , with narrow  $E_p^s$  range (one order of magnitude). Then the Amati correlation ( $E_p \propto E_{iso}^{1/2}$ ) is reproduced over three orders of magnitude in  $E_p$ . Although the scatter around the Amati correlation is large in the simulation, the results are consistent with the observed properties of GRBs with known redshifts and the BATSE GRBs with pseudo redshifts derived from the lag-luminosity correlation. We argue that for brighter bursts the Amati correlation arises from intrinsic property, while for dimmer bursts it arises from the off-axis effects of multiple emissions. The intrinsic  $E_p^s \propto L_{iso}^s{}^{1/2}$  correlation is supported by the observations (Liang, Dai, & Wu 2004; Lloyd-Ronning & Ramirez-Ruiz 2002) and could be derived in the context of standard synchrotron internal shock model.

*HETE* team defines XRRs and XRFs as those events for which  $\log[S_X(2-30 \text{ keV})/S_\gamma(30-400 \text{ keV})] > -0.5$  and  $0.0$ , respectively (Lamb et al. 2004). We calculate the observed fluence ratio for simulated bursts surviving the peak flux truncation, and classify them into GRBs, XRRs, and XRFs. The ratio of the simulated event rate is  $R_{GRB} : R_{XRR} : R_{XRF} \sim 4 : 3 : 1$ . *HETE-2* observations show similar number of GRBs, XRRs, and XRFs (Sakamoto et al. 2005). We can say that the event rate among GRBs, XRRs and XRFs is consistent with the observations. Figure 5 shows the redshift distribution of GRBs (the solid line), XRRs (the dashed line) and XRFs (the dot-dashed line). The mean redshifts of GRBs, XRRs and XRFs are 1.9, 3.2, and 2.3, respectively. XRRs have a little larger redshifts than GRBs and XRFs. Figure 2 plots the viewing angles for detectable XRFs, which are represented by plus signs. We see that the main population of the XRFs arises from the off-axis effects. On the other hand, many XRRs are on-axis events. Since  $E_p > 200 \text{ keV}$  for on-axis events in our simulation, the on-axis XRRs arise from the cosmological redshift effect. The ratio of the on-axis and off-axis XRRs is  $\sim 1 : 1$ . We expect that the event rate ratio from larger observed samples will give us some information about the angular distribution of the subjets within the whole GRB jet and the redshift distribution of the GRB sources.

In this paper, we have performed the simulations with fixed Lorentz factor of the subjets,  $\gamma = 300$ . As discussed in § 4, the range of the index  $a$  of the  $E_p$ - $E_{iso}$  correlation for off-axis events is independent of the Lorentz factor. We perform the same simulations in the case (ii) for  $\gamma = 100$  and  $500$ , and obtain the Amati correlation ( $E_p \propto E_{iso}^{1/2}$ ) through all bursts. However, the peak photon flux of the XRF is small for lower Lorentz factor. For  $\gamma = 100$ , we obtain  $R_{GRB} : R_{XRR} : R_{XRF} \sim 15 : 10 : 1$ . Alternatively for  $\gamma = 500$ ,  $R_{GRB} : R_{XRR} : R_{XRF} \sim 3 : 2 : 1$ .

Figure 6 shows the distribution of the  $T_{90}$  durations in the 50–300 keV band for GRBs (solid line), XRRs (dashed line),

and XRFs (dot-dashed line). GRBs have a bimodal distribution as observed by BATSE. We have already shown why GRBs have the bimodal duration distribution in our multiple subjet model (Toma, Yamazaki, & Nakamura 2005): the  $T_{90}$  duration of an  $n_s = 1$  burst is determined by the width of a single pulse, while that of an  $n_s \geq 2$  burst is determined by the time interval between the observed first pulse and the last one. These two different timescales naturally lead to a division of the burst  $T_{90}$  durations into the short and long ones. We also calculate the distribution of the  $T_{90}$  durations in the 2–25 keV band. Figure 7 shows the result. These distributions are not inconsistent with the *HETE-2* data (see Fig. 4 of Sakamoto et al. 2005). The  $T_{90}$  durations of  $n_s = 1$  bursts (i.e., short bursts) become larger when they are measured in the softer band, since soft emission from the periphery of the subjet is observed for a longer time. Yamazaki, Ioka, & Nakamura (2004b) have predicted short XRRs in our unified model, which are confirmed in this simulation. These are events of a single subjet viewed off-axis or viewed on-axis with slightly high redshift. Indeed, GRB 040924 may be an example of short XRRs, from which recent HST observation reveals the supernova signature (Soderberg et al. 2005). This event supports our unified picture.

In this paper, we considered the  $\theta^{-2}$ -angular distribution of the subjets. Averaging by a solid angle satisfying  $(\Delta\theta_{\text{sub}})^2 < \Omega < (\Delta\theta_{\text{tot}})^2$ , the distribution of the emission energy (or almost equivalently the angle-averaged kinetic energy) is the same as the universal structured jet model (Rossi, Lazzati, & Rees 2002; Zhang & Mészáros 2002a). The universal structured jet model has been criticized by Lamb, Donaghy, & Graziani (2005): in the universal structured jet model, it is assumed that XRFs are observed when the jet is viewed from fairly large angle, so that the model overpredicts the number of XRFs, which is inconsistent with the observed ratio of the number of XRFs and GRBs detected by *HETE-2*. Then, Zhang et al. (2004) modified the universal structured jet model, and showed that if the jet is structured with a Gaussian-like shape, the number of XRFs becomes small. In these works it is assumed that the jet is continuous and there are no cold spots inside the jet. As shown in this paper, Eichler & Levinson (2004), and Yamazaki, Ioka, & Nakamura (2004b), if the observer points toward the cold spot (i.e.,  $n_s = 0$ ), XRFs or XRRs are observed. While if  $n_s \geq 2$ , the event looks like a long GRB irrespective of the viewing angle. In our model, the ratio of the total solid angle with  $n_s \geq 2$  and  $n_s = 0$  determines the event rate of GRBs and XRRs/XRFs. Interestingly, we find that the power-law profile with an index of  $-2$  is preferable to the Gaussian profile in order to reproduce the ratio of observed event rate of GRBs, XRRs, and XRFs, because the solid angle with  $n_s = 0$  is small in the Gaussian profile. Lazzati & Begelman (2005) have recently argued that in the context of the collapsar model,  $\theta^{-2}$  angular profile might be obtained as a consequence of the physics in the jet breakout irrespective of the jet structure inside the progenitor. From the observational side, we can estimate the pseudo jet opening angle distribution. Using the Ghirlanda correlation ( $E_p \propto E_\gamma^{0.71}$ ) where  $E_\gamma = E_{iso}\theta_j^2/2$  (Ghirlanda, Ghisellini, & Lazzati 2004) and the Yonetoku correlation ( $E_p \propto L_p^{0.5}$ ) where  $L_p$  is a peak luminosity (Yonetoku et al. 2004), Yonetoku et al. (2005) obtained that the pseudo jet opening angle obeys  $f(\theta_j)d\theta_j \propto \theta_j^{-2}d\theta_j$ . This is compatible with the power-law structured jet

model: if all bursts were observable, the distribution would be uniform per unit solid angle and  $f(\theta) \propto \theta$ . However  $E_{iso}$  for the smaller viewing angle is brighter by a factor of  $\theta^{-2}$ , so that the maximum observable distance is larger by a factor of  $\theta^{-1}$  which contains a volume larger by a factor of  $\theta^{-3}$ . Then we have  $f(\theta) \propto \theta^{-2}$ .

Late phase evolution of a set of multiple subjects is rather complicated and hard to be predicted. Cold spots do not produce high energy emission but may be filled with the kinetic energy that is not dissipated at small radius (see also Levinson & Eichler 2005). Even if cold spots are not filled with the kinetic energy, all subjects begin to expand sideways and would merge into one shell. In any case, late afterglow behavior may be well approximated by the results from the continuous structured jet model (e.g., Kumar & Granot 2004). As shown in Fig. 2, almost all XRFs arise when all the subjects are viewed off-axis, i.e.,  $n_s = 0$ , while the observers see the whole jet on-axis. Then, the late phase ( $\gtrsim 1$  day) properties of XRF

afterglows may not be like orphan afterglows but may show similar behavior to those of normal GRBs (e.g., Amati et al. 2004). On the other hand, as rare cases, when the whole jet is viewed off-axis, XRF afterglows may resemble the orphan afterglow (e.g., Granot, Ramirez-Ruiz, & Perna 2005). XRF 030723 may be a member of such a class (Butler et al. 2005; Fynbo et al. 2004).

We are grateful to the referee for useful comments. K. T. thanks M. Ohashi for helpful discussion. This work is supported in part by the Grant-in-Aid for the 21st Century COE ‘‘Center for Diversity and Universality in Physics’’ from the Ministry of Education, Culture, Sports, Science and Technology (MEXT) of Japan and also by Grants-in-Aid for Scientific Research of the Japanese Ministry of Education, Culture, Sports, Science, and Technology 09245 (R. Y.), 14047212 (T. N.), 14204024 (T. N.) and 17340075 (T. N.).

## REFERENCES

- Amati, L. et al. 2002, *A&A*, 390, 81  
 Amati, L. et al. 2004, *A&A*, 426, 415  
 Band, D. L., et al. 1993, *ApJ*, 413, 281  
 Band, D. L. 2003, *ApJ*, 588, 945  
 Butler, N. R., et al. 2005, *ApJ*, 621, 884  
 Eichler, D., & Levinson, A. 2004, *ApJ*, 614, L13  
 Fynbo, J. P. U., et al. 2004, *ApJ*, 609, 962  
 Ghirlanda, G., Ghisellini, G., & Lazzati, D. 2004, *ApJ*, 616, 331  
 Ghirlanda, G., Ghisellini, G., & Firmani, C. 2005a, *MNRAS*, 361, L10  
 Ghirlanda, G., Ghisellini, G., Firmani, C., Celloti, A., & Bosnjak, Z. 2005b, *MNRAS*, 360, L45  
 Granot, J., Ramirez-Ruiz, E., & Perna, R., 2005, preprint (astro-ph/0502300)  
 Ioka, K., & Nakamura T. 2001, *ApJ*, 554, L163  
 Ioka, K., & Nakamura, T. 2002, *ApJ*, 570, L21  
 Kumar, P., & Piran, T. 2000, *ApJ*, 535, 152  
 Kumar, P. & Granot, J. 2004, *ApJ*, 591, 1075  
 Lamb, D. Q., et al. 2004, *NewA Rev.*, 48, 423  
 Lamb, D. Q., Donaghy, T. Q., & Graziani, C. 2005, *ApJ*, 620, 355  
 Lazzati, D. & Begelman, M. C. 2005, preprint (astro-ph/0502084)  
 Levinson, A. & Eichler, D. 2005, preprint (astro-ph/0504125)  
 Liang, E. W., Dai Z. G., & Wu, X. F. 2004, *ApJ*, 606, L29  
 Lloyd-Ronning, N. M., & Ramirez-Ruiz, E. 2002, *ApJ*, 576, 101  
 Nakamura, T. 2000, *ApJ*, 534, L159  
 Porciani, C., & Madau, P. 2001, *ApJ*, 548, 522  
 Rossi, E., Lazzati, D., & Rees, M. J. 2002, *MNRAS*, 332, 945  
 Sakamoto, T., et al. 2005, *ApJ*, 629, 311  
 Soderberg, A. M., et al. 2005, preprint (astro-ph/0504359)  
 Toma, K., Yamazaki, R., & Nakamura, T. 2005, *ApJ*, 620, 835  
 Woods, E. & Loeb, A. 1999, *ApJ*, 523, 187  
 Yamazaki, R., Ioka, K., & Nakamura, T. 2002, *ApJ*, 571, L31  
 Yamazaki, R., Ioka, K., & Nakamura, T. 2003, *ApJ*, 593, 941  
 Yamazaki, R., Ioka, K., & Nakamura, T. 2004a, *ApJ*, 606, L33  
 Yamazaki, R., Ioka, K., & Nakamura, T. 2004b, *ApJ*, 607, L103  
 Yonetoku, D., Murakami, T., Nakamura, T., Yamazaki, R., Inoue, A. K., & Ioka, K. 2004, *ApJ*, 609, 935  
 Yonetoku, D., Yamazaki, R., Nakamura, T., & Murakami, T. 2005, preprint (astro-ph/0503254)  
 Zhang, B., & Mészáros, P. 2002a, *ApJ*, 571, 876  
 Zhang, B., & Mészáros, P. 2002b, *ApJ*, 581, 1236  
 Zhang, B., Dai, X., Lloyd-Ronning, N. M., & Mészáros, P. 2004, *ApJ*, 601, L119

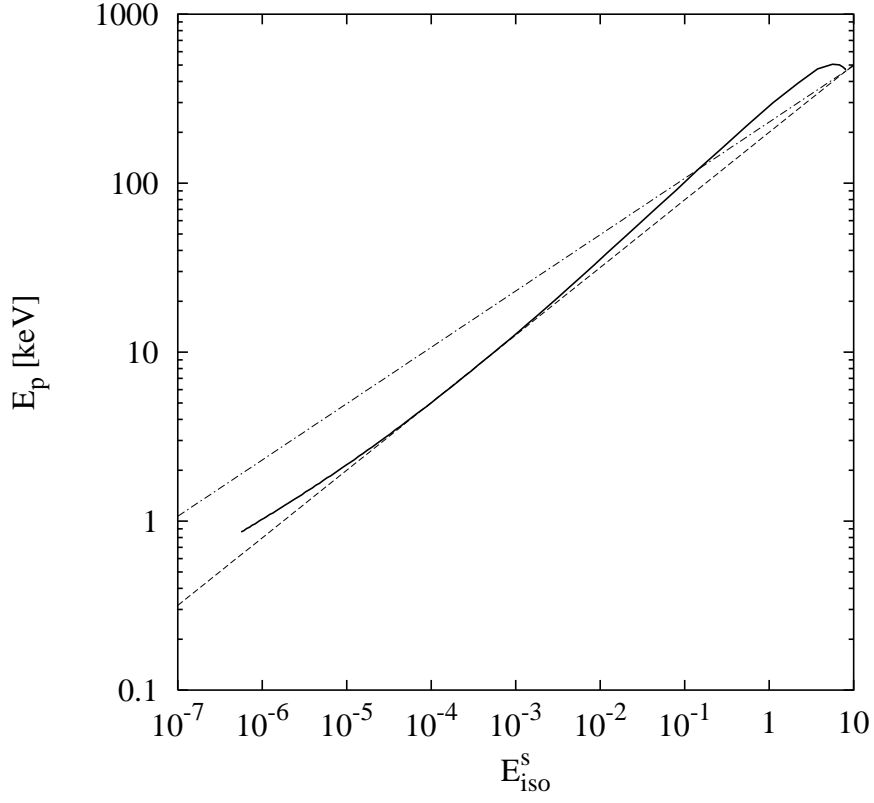


FIG. 1.— Correlation between the isotropic-equivalent energy  $E_{iso}^s$  (in units of  $2.8 \times 10^4 \pi A r_0^2$ ) and the spectral peak energy  $E_p$  for a single subset.  $E_{iso}^s{}^{0.4}$  (dashed) and  $E_{iso}^s{}^{1/3}$  (dot-dashed) lines are also shown.

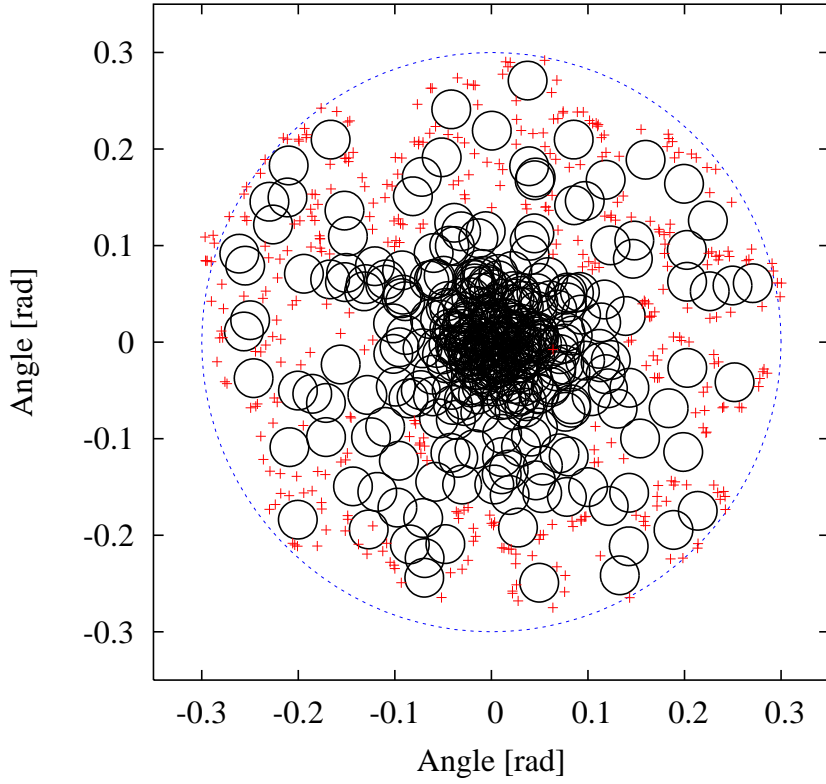


FIG. 2.— Angular distribution of  $N_{\text{tot}} = 350$  subjects confined in the whole GRB jet in our simulation. Each subject is located according to the power-law distribution function of eq.(8). The whole jet has an opening half-angle of  $\Delta\theta_{\text{tot}} = 0.3$  rad. The subjects have the same opening half-angles of  $\Delta\theta_{\text{sub}} = 0.02$  rad. The angular size of the subjects are represented by the solid circles, while the whole jet is represented by the dashed circle. The viewing angles for detectable XRFs in our simulation are represented by plus signs.

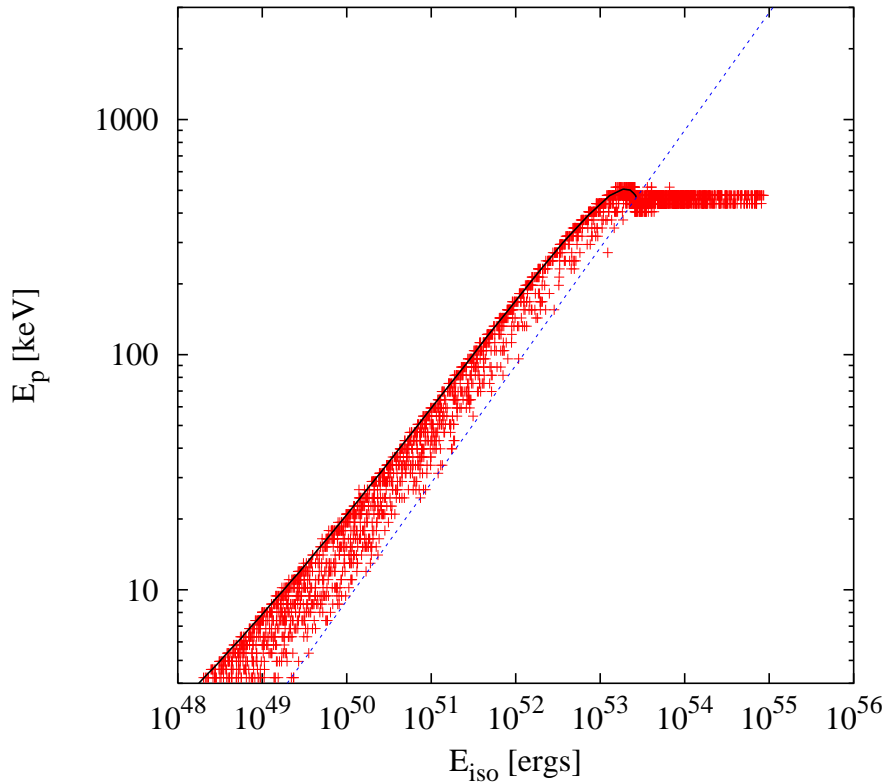


FIG. 3.—  $E_p$ - $E_{iso}$  diagram in the multiple subject model in which all the properties of each subject are the same. The simulated bursts are represented by plus signs.  $E_p$ - $E_{iso}$  line for a single subject is described by solid line. The dashed line is  $(E_p/1 \text{ keV}) = 90(E_{iso}/10^{52} \text{ ergs})^{1/2}$ .

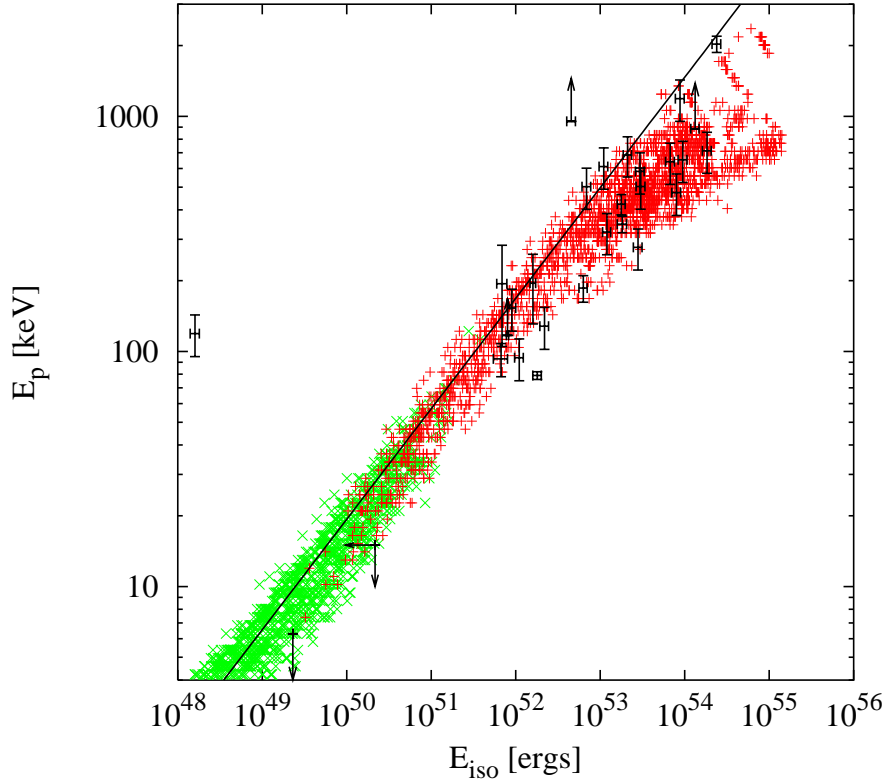


FIG. 4.— Same as Figure 3, but in the multiple subjet model in which subjet parameters  $\gamma\nu_0^{(j)}$ ,  $A^{(j)}$ , and  $\xi$  are distributed (see text for details). Plus signs represent bursts that can be detected by *HETE-2*, while crosses represent ones that cannot be detected. They are compared with the *BeppoSAX* and *HETE-2* data (points with error bars) taken from Ghirlanda, Ghisellini, & Lazzati (2004). The solid line represents the best fitted line for 442 GRBs with redshifts estimated by the lag–luminosity correlation (Ghirlanda, Ghisellini, & Firmani 2005a).

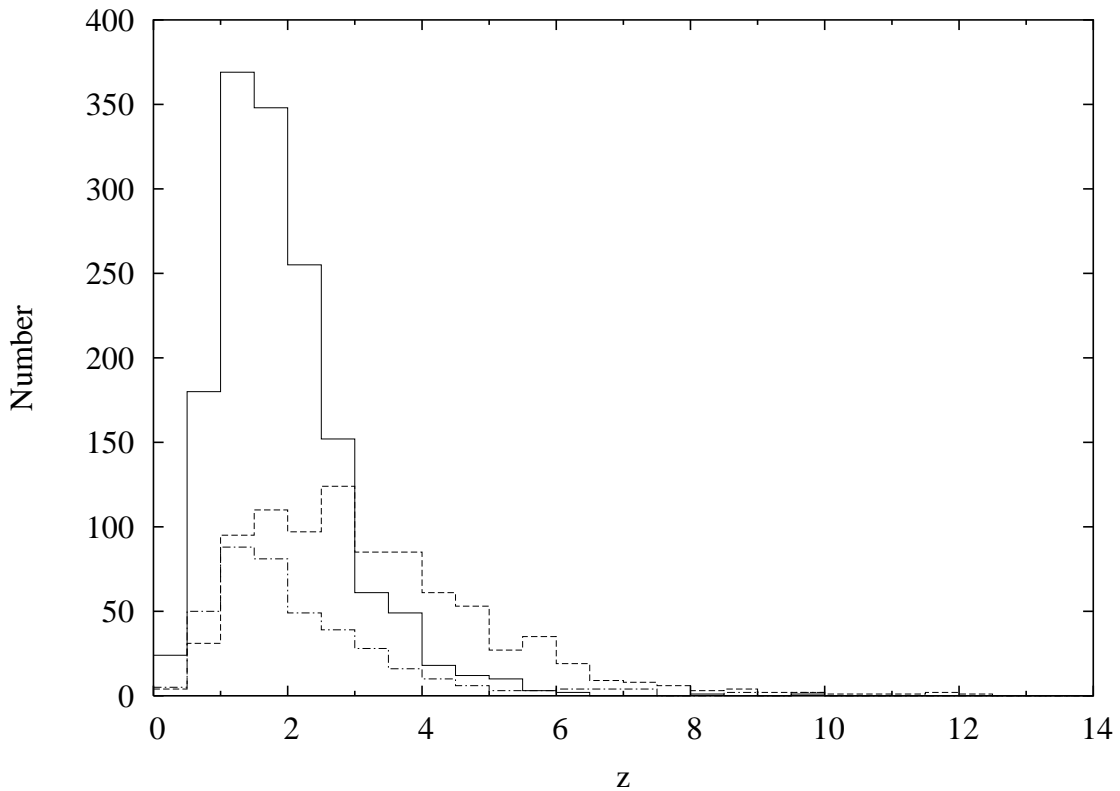


FIG. 5.— Redshift distribution of the simulated bursts surviving the peak photon flux truncation. Solid line, dashed line, and dot-dashed line represents the distribution for GRBs, XRRs, and XRFs, respectively.



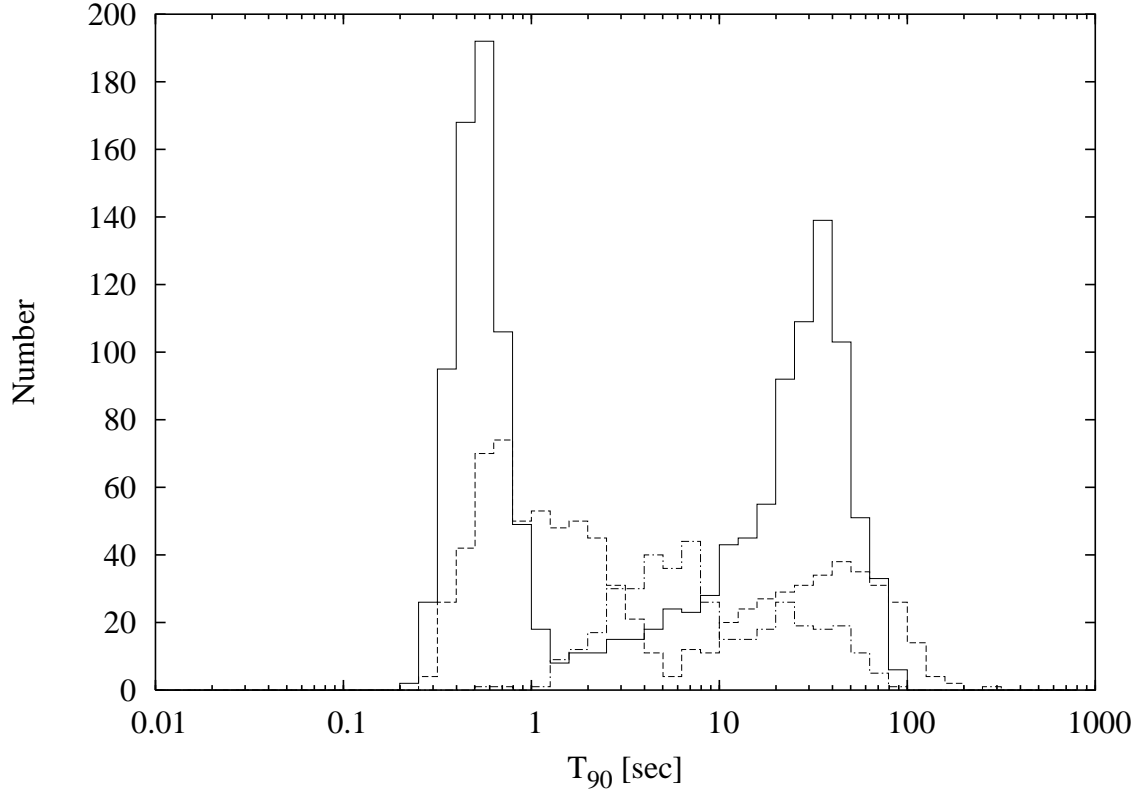


FIG. 6.— Distribution of the  $T_{90}$  durations in the 50–300 keV band of the simulated bursts surviving the peak flux truncation. Solid line, dashed line, and dot-dashed line represents the distribution for GRBs, XRRs, and XRFs, respectively.

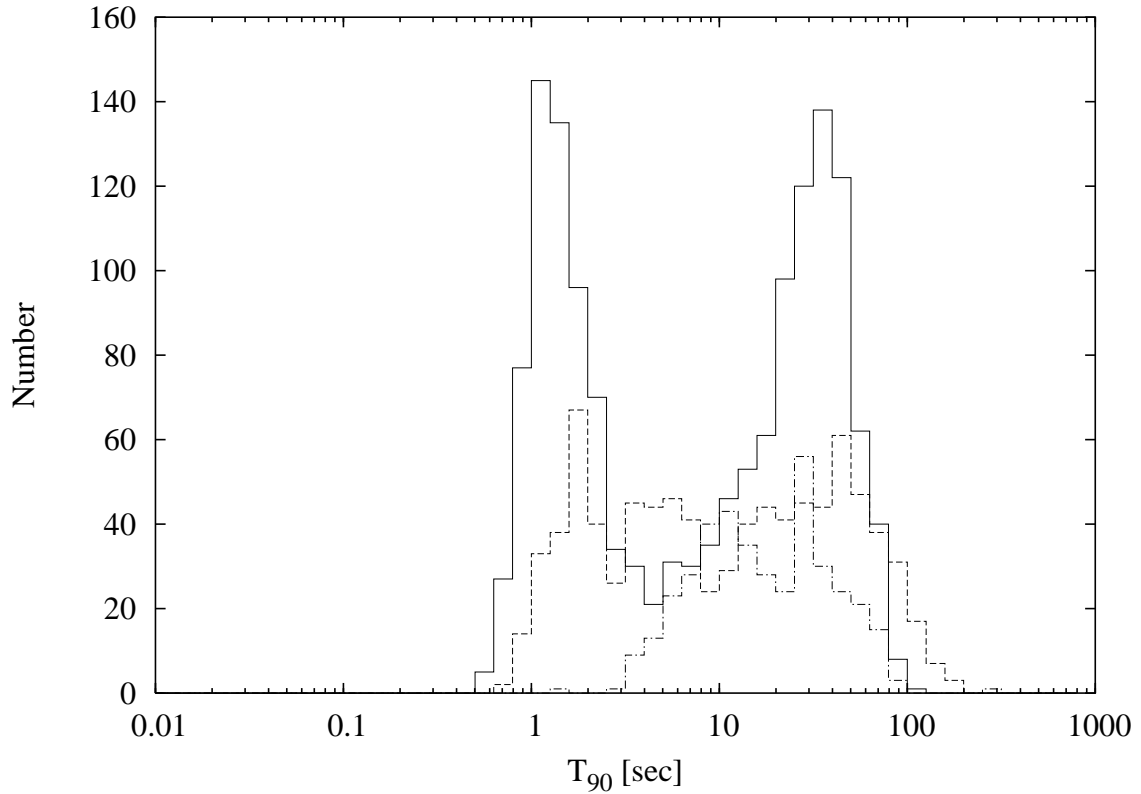


FIG. 7.— Distribution of the  $T_{90}$  durations in the 2–25 keV band of the simulated bursts surviving the peak flux truncation. Solid line, dashed line, and dot-dashed line represents the distribution for GRBs, XRRs, and XRFs, respectively.